arXiv:2501.18851v3 [cs.CV] 2 May 2025

# Project-and-Fuse: Improving RGB-D Semantic Segmentation via Graph Convolution Networks

Xiaoyan Jiang[1,2], Bohan Wang[1], Xinlong Wan[1], Shanshan Chen[1], Hamido Fujita[3, 4, 5*], Hanan Abd. Al Juaid[3]

[1]Shanghai University of Engineering Science, Shanghai, 200000, China.
[2] Leiden University, Leiden, EZ 2311, Netherlands.
[3] Princess Nourah bint Abdulrahman University, Riyadh, 13412, Saudi Arabia.
[4]Malaysia-Japan International Institute of Technology, Universiti Teknologi Malaysia, Kuala Lumpur, 54100, Malaysia.
[5]Regional Research Center, Iwate Prefectural University, Takizawa, 020-0693, Japan.

*Corresponding author(s). E-mail(s): fujitahamido@utm.my;
Contributing authors: xiaoyan.jiang@sues.edu.cn; adeclaire18@gmail.com; Ke-Ji666@outlook.com; sschen33@sues.edu.cn; haaljuaid@pnu.edu.sa;

**Abstract**

Most existing RGB-D semantic segmentation methods focus on the feature level fusion, including complex cross-modality and cross-scale fusion modules. However, these methods may cause misalignment problem in the feature fusion process and counter-intuitive patches in the segmentation results. Inspired by the popular pixel-node-pixel pipeline, we propose to 1) fuse features from two modalities in a late fusion style, during which the geometric feature injection is guided by texture feature prior; 2) employ Graph Neural Networks (GNNs) on the fused feature to alleviate the emergence of irregular patches by inferring patch relationship. At the 3D feature extraction stage, we argue that traditional CNNs are not efficient enough for depth maps. So, we encode depth map into normal map, after which CNNs can easily extract object surface tendencies. At projection matrix generation stage, we find the existence of Biased-Assignment and Ambiguous-Locality issues in the original pipeline. Therefore, we propose to 1) adopt the Kullback–Leibler Loss to ensure no missing important pixel features, which can be viewed as hard pixel mining process; 2) connect regions that are close to

each other in the Euclidean space as well as in the semantic space with larger edge weights so that location informations can been considered. Extensive experiments on two public datasets, NYU-DepthV2 and SUN RGB-D, have shown that our approach can consistently boost the performance of RGB-D semantic segmentation task.

**Keywords:** RGB-D, semantic segmentation, GCN, late fusion

# 1 Introduction

Semantic segmentation refers to the pixel-wise classification of images, which plays an important role in scene understanding, medical image analysis, robot perception, etc[1]. It is well-known that classic Convolutional Neural Networks have excelled at capturing local texture features compared with traditional methods. But considering that the patch from one corner may be related to the patch from another corner, it is necessary for CNNs to have larger receptive field which enables it to capture the long-range dependencies. To enable the CNNs to recognize patterns in a larger scale, the previous solutions are to design various convolutional architectures [2] or concatenate multiple kernels [3] to have larger receptive field; later, the attention-based methods [4] [5] introduce the attention score to capture dependencies and fusion-based methods [6] [7] propose to fuse features at different stages so as to aggregate multi-scale semantics; more recently, transformers-based methods [8][9] have excelled at various computer vision tasks. However, most of these methods always come with the massive number of parameters, and how to precisely extract multi-scale semantic dependencies in a more effective as well as explainable way remains to be further studied.

Indoor semantic segmentation is one of the most challenging problems due to the complex layouts and various occlusions [10]. The popularity of depth sensors in recent years has made it easy to capture depth map along with the RGB-D images, which further boost the research relevant to multi-modal fusion. There are three popular pipelines to fuse RGB and depth data based-on when the fusion happens. Early fusion, known as input-level fusion, refers to combine two modalities before any feature extraction operations. Middle fusion is also called as feature-level fusion, meaning that features from different modalities are aggregated during the feature learning stage, which have been studied in various approaches. Late fusion is also named as decision-level fusion, referring to the fusion happened after feature extraction.

Despite various methods proposed in recent years have greatly improved the accuracy of RGB as well as RGB-D semantic segmentation, the results are still not good enough. Specifically, there still exists irregular patches which are unreasonable for human beings and can be easily rectified with a little human's common sense. Fig 1 shows some cases that are very counter-intuitive for a reasonable human being, but for the neural networks, it is hard to distinguish the relations between different classes.

Some works tried to solve the above counter-intuitive segmentation problem. [11] presents intra-class and inter-class reasoning to exploit dependency relations among visual entities. To achieve a holistic understanding of an image, [12] incorporates graph

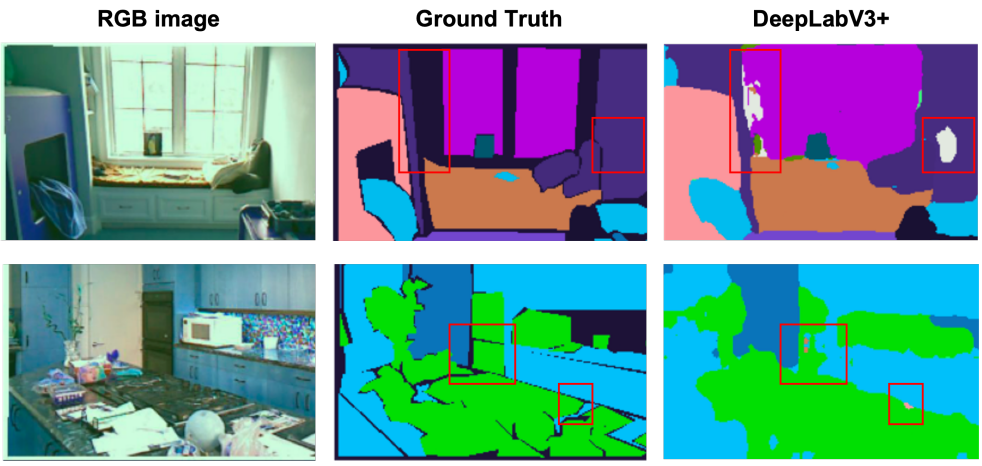


**Fig. 1** The counter-intuitive cases. Existing segmentation results exist scenes that are against human's commonsense. The first row shows that there exist toilet(white) next to the window(purple), and the second row shows there exist emerge a small patch of ceiling in the middle of shelves.

structure into the conventional segmentation networks and explicitly model the correlations between object and background. Similarly, researchers in other computer vision tasks noticed the importance of relations between entities. Authors in [13] tried to learn the relations via graph reasoning on a knowledge graph for the object detection. [14] explores the relationship between regions rather than pixels considering that regions have richer semantics than pixels.

We extract commonalities among the previous graph-based reasoning networks and summarize them into a pipeline, as shown in fig 2 (a). To solve the counter-intuitive errors in RGB-D indoor semantic segmentation tasks, as Fig 2 (b) shows, we seamlessly inject the 3D branch into this pipeline and fuse two modalities in a texture-prior style. In practice, we found that the assignment are not effective and positional properties are completely ignored during the graph construction process. This leads to the loss of valuable semantic and positional features and further hurts the final performance. Therefore, we add two constraints on the projection matrix and changed the way how adjacent matrix is generated. Experiments shows the effectiveness of these modifications.

The main contributions are summarized as follows:

1. To effectively solve the "irregular patch" errors in RGB-D semantic segmentation, we propose to upgrade the existing pixel-node-pixel pipeline with the addition of a 3D branch, during which features from two modalities are fused in a texture-prior style.

2. To alleviate the Biased-Assignment and Ambiguous-Locality problem in graph construction process, we add constraints on the projection matrix and changed the way how adjacent matrix is generated.

3. Extensive experiments on NYU-v2 and SUN RGB-D show that the proposed approach achieve competitive state-of-the-art performance.

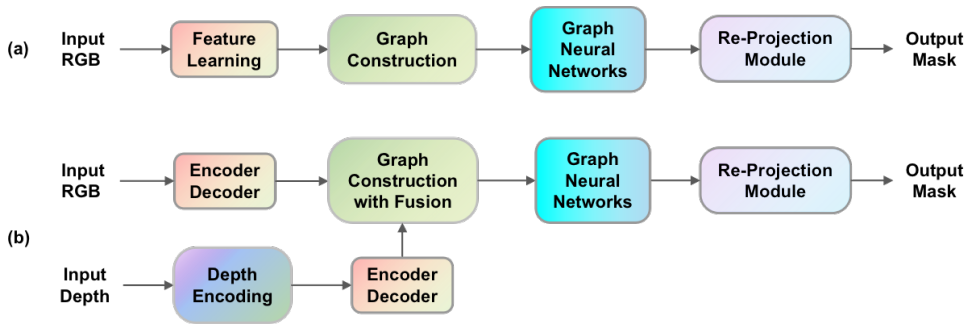


**Fig. 2** (a) The popular pixel-graph-pixel networks pipeline, which is mainly composed of four modules: feature extraction and representation learning as most backbones do; graph construction based on the learned feature maps, graph representation updating via various graph neural networks; graph re-projection to transform graph back to the feature map. (b) The proposed fusion pipeline. We encode the depth map so that 3D features can be better captured by CNNs. The original pipeline is updated to modal fusion so that complementary information can be aggregated.

# 2 Related Works

## 2.1 2D Semantic Segmentation

For 2D Semantic segmentation, the traditional way is to use random forest and conditional random field (CRF) to segment masks. The deep learning-based methods [15] has started a new era of segmentation models, and the encoder-decoder architecture has become the mainstream solution in semantic segmentation tasks[16]. DeepLab series [17][18] introduce Dilated Convolution and Atrous Spatial Pyramid Pooling Module to equip the network with larger receptive field, which enables the network to fuse multi-scale features and no longer limited by the size of the input image.

Meanwhile, the combination of computer vision and attention mechanism has also made networks learn long-range dependencies and improved the performance on semantic segmentation tasks. [19] computes the response at a position as a weighted sum of the features at all positions in order to connect different positions. Instead of capturing contexts by multi-scale features fusion, [20] presents a Dual Attention Networks (DANet) to adaptively integrate local features with their global dependencies. [21] presents a Criss-Cross Network (CCNet) to obtain full-image contextual information in a very effective and efficient way.

In summary, on one hand, there exists delicate balance between global feature and local feature selection when determining the class to which a pixel belongs. On the other hand, as the network goes deeper, the increasing computational complexity made it difficult to be deployed in practical industrial applications.

## 2.2 3D Semantic Segmentation

As the acquisition of 3D sensors become easier, research on RGB-D semantic segmentation [10] leads to the question of how to integrate data from different modalities. It is generally accepted that CNNs designed for RGB images and depth maps should be different from each other due to the variations between the two modalities.

Many methods take RGB-D semantic segmentation as a fusion task. Based on the time fusion, it can be categorized as early-fusion, middle-fusion, late-fusion, and hybrid fusion [22]. Early-fusion is also called "input-level" fusion. Authors in [23] multiply RGB data with a depth-relevant weight matrix before feeding it into the network. [24] is a simple example of incorporating depth feature into an encoder-decoder segmentation framework. [25] feed RGB and depth data into two parallel CNN streams and fuse the feature map via multi-modal feature fusion blocks and multi-level feature refinement blocks. [26] propose to adaptively merge RGB and depth according to their weighted contributions at the decision-level. [27] utilize the magnitude of Batch-Normalization (BN) scaling factor to exchange "more useful" features.

Although these fusion-based methods achieve competitive segmentation results, there still exists two main problems: the interpretability of the fusion process and the misalignment issue. On one hand, these well-designed fusion modules are usually based upon two parallel CNN streams. Complex fusion mechanism usually leads to poor interpretability. On the other hand, as [28] describes, when the network goes deeper, the size of feature map decreases and the semantics becomes more abstract. Thus, a simple element-wise addition or concatenation in the feature extracting process may not only cannot fully utilize the complementary information, but also result in misalignment issue.

It is commonly acknowledged that RGB images have rich photometric features while depth maps only depict the distances from object surfaces to the camera which are relatively texture-less. We argue that depth maps have two kinds of valuable information: the edges, indicating there is a gap between neighboring pixels; the tendencies, depicting the 3D surface features. There are also many methods design geometric-aware convolution kernels to jointly process RGB and depth data and alleviate the gap between two modalities. [29] seamlessly incorporate geometry into CNN via a depth-aware convolution and a depth-aware average pooling, during which no additional parameters introduced. [30] present an operator called malleable 2.5D convolution to learn the receptive field along the depth-axis. Authors in [31] consider the shape as a more inherent attribute to the semantics, and introduce shape-aware convolutional layer to process the depth feature. Theoretically innovative as these methods are, they cannot cover all the complex indoor layouts, which lead to dissatisfied results.

More recently, methods that taking RGB-D semantic segmentation as a distillation task or introducing transformer modules have also achieved competitive results. [32] propose to jointly infer two modalities information by distilling geometry-aware embedding and use the learned embedding to improve segmentation result. [33] distill 3D knowledge from a pre-trained 3D network to supervise a 2D network and calibrate the 2D and 3D features for better integration via a two-stage dimension normalization. [34] calibrate the feature of two modalities in spatial-wise and channel-wise dimensions via a Cross-Modal Feature Rectification Module (CM-FRM), and deploy a Feature Fusion Module (FFM) in a cross-attention style to mix features from different modalities for the final semantic prediction.

To summarize, the difficulties for the RGB-D semantic segmentation task are as follows. 1) the misalignment issues and feature selection bias when middle-fusion happens, which may introduce unnecessary trouble; 2) the trade-off between better

results and larger network parameters, which is an important consideration when applied to industrial applications.

### 2.3 Graph Neural Networks in Computer Vision

The GNN are originally used to handle irregular-structured data, such as, molecular structure, social networks, and etc., to capture structural relations. In recent years, the graph neural networks (GNNs) in the application of computer vision has drawn a lot of attention, such as, person recognition [35], object detection [36][37][38], and etc.

For RGB-D semantic segmentation, there are methods directly design GNNs to solve the per-pixel classification problem. [39] introduce a 3D graph neural network (3DGNN) to build a k-nearest neighbor graph on a set of 3D point-cloud converted from depth data. Each node dynamically updates its hidden feature based on its own status and messages from its neighbors, and the final per-node representation is used for semantic class predicting of each pixel. [40] present a 3D Neighborhood convolutions by modeling the receptive field of the 2D convolution in accordance with the 3D local neighborhood. It is the first concept framework to explicitly cover both the scale and the locality from depth in theory, which learns better 3D-aware features.

There are also some methods try to capture abstract semantic relations via Graph Neural Networks [41][42][43]. As Fig 2 (a) shows, the pipeline can be summarized into 3 steps: 1) map the features from coordinate space to hidden interaction space to construct a semantic-aware graph, 2) perform reasoning on the graph and update node features, 3) map the graph back to the coordinate space and get the updated feature map. Most methods differ in the first two steps: how to construct a graph from the feature map and how to perform message passing to update node features.

Specifically, [41] generate the nodes based on the similarity between different pixels, known as regions, and the edges of the graph represent the similarity between different regions. To propagate information on the learned graph, the graph convolutional networks is used [44], during which the reasoning go beyond the traditional regular grids and captured long-range dependencies among different regions. [42] propose a new Symbolic Graph Reasoning (SGR) layer to perform reasoning over a group of symbolic nodes, aiming to explicitly represent different semantics in a prior knowledge graph. [43] present a lightweight yet highly efficient unit names as Global Reasoning unit, which achieved the coordinate-interaction space mapping via weighted global pooling and weighted broadcasting, and the relation reasoning via graph convolution on a small graph in interaction space.

More recently, there are also some inspiring research. [45] propose to represent the image via a graph structure and introduce a vision GNN (ViG) architecture to extract graph-level features for visual tasks. Instead of measuring the semantic consistency as the weight of edges, ViG connects nodes based on the nearness, which conserved the locality of original space. To address the over-smoothing problem and the high-cost at high-level problem, [46] design a topology of GNNs in a novel feature fusion perspective and propose a neural architecture search method which contains a set of feature selection and fusion operations.

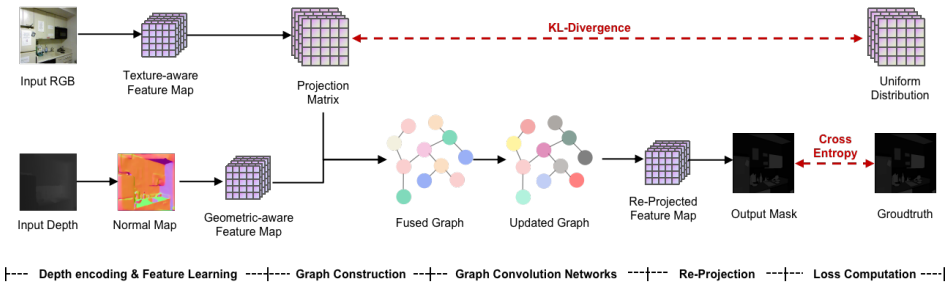


**Fig. 3** Details of the proposed approach. We first encode the depth map into normal map, so that the two modalities can be sent into parallel feature extraction branches. Graph construction module takes two feature maps as its input and output the fused graph. Pixels that have similar semantics and localities are marked as a region and assigned to the same node. The similarities between two regions are considered to generate the edge weights. Afterward, graph neural networks are adopted to update node features. Finally, updated node feature are back-projected to the feature map.

In summary, these approaches all point out the importance of semantic correlation between regions and use GNN to extract semantic features, ultimately achieving better feature extraction performance that are beneficial for the downstream tasks. But in practice, there exists two main problems, namely Biased-Assignment and Ambiguous-Locality. First, as training goes, the soft-assignment projection matrix tends to assign some pixels to multiple nodes while other pixels to no nodes, resulting GNNs pay redundant attentions to some region while almost none to others. We call this phenomenon Biased-Assignment issue. Second, these methods measure region connectivity solely based-on the semantic similarity, but in semantic segmentation task, the location of each pixel do have a decisive impact on the final prediction.

# 3 The proposed method

## 3.1 Overview

The overall structure of the proposed network is shown in Fig 3. Detailed module design and the loss function are illustrated in the following sections. Our highlights are mainly at depth encoding module and graph construction module: 1) to better handle the depth map with CNNs, we propose to transform one-channel depth map to three-channel normal map; 2) to efficiently and effectively fuse features of the two modalities, the texture-oriented projection matrix and a summation operation are used for seamless feature fusion; 3) to alleviate the Biased-Assignment issue, we add a constraint on the projection matrix. The KL-loss is proposed to force the assignment score of the graph to be evenly distributed; 4) to embed positional information into the graph, we generate adjacent matrix based-on the Euclidean distance at graph construction stage.

## 3.2 Data Pre-Processing

The data pre-process module takes data from two modalities as input and output the initial feature map for the following fusion and processing. This module is composed

of two branches: main 2D branch and injected 3D branch, both of which adopt the popular encoder-decoder based segmentation networks, i.e. DeepLabV3+, to get the preliminary feature map.

For 3D branch, due to the inherently difference between RGB and depth data, as [31] mentioned, the convolution operator that is widely adopted for RGB data might not be the optimal for the depth map processing. To enable the network to better handle such features and the subsequent fusion operation, we encode the depth map into normal map as the input of 3D branch. Considering the different complexity of the two modalities, the backbone of 3D branch is relatively simpler, i.e., ResNet50 for 2D branch and ResNet18 for 3D branch. Experiments in 4.3 shows such settings doesn't hurt the final performance.

In this section, we will describe how to encode the single-channel depth map to the three-channel normal map. As previous method [47] described, with the camera parameters and depth data, we can project the depth map as a set of point cloud and compute the normal vector based on the neighborhood region of the point. The depth encoding process can be seen in Fig 4(a).

### 3.2.1 Pinhole Camera Model

In order to project depth map as a set of point cloud, we adopt the pinhole camera model. For the pixel $(u_i, v_i)$ in the depth map, its corresponding location in 3D space $s_i : (x_i, y_i, z_i)$ can be obtained by

$$\begin{aligned} x_i &= (u_i - c_x) * z_i / f_x \\ y_i &= (v_i - c_y) * z_i / f_y \end{aligned} \tag{1}$$

where $z_i$ is the depth value; $f_x$ and $f_y$ are the focal length along with $x$ and $y$ directions, respectively; $c_x$ and $c_y$ are coordinates of the principal points. Note that $f_x$, $f_y$, $c_x$ and $c_y$ are camera-relevant parameters and have been given along with the depth maps. Here, we get the point set $S = \{s_1, s_2, ..., s_i, ..., s_{H*W}\}$, which will be used not only in the up-coming normal vector computing process, but also in the edge weights generation module.

### 3.2.2 Neighborhood Defining

In order to compute the surface normal vectors at pixel $i$, we need to determine its tangent plane, which can be determined in $x$, $y$ and $z$ directions. Specifically, given the target point $s_i : (x_i, y_i, z_i)$, we define its top-k nearest are $N_i^k := \{s_1, s_2, ..., s_k\}$ based on the Euclid distance computing. But considering the depth gaps between nearby pixels may harm the accuracy of final normal vector output, we add an regulation term: $|z_i - z_j| < \gamma * z_i$. So far, we get $s_i$'s k-nearest neighbor set $N_i^k$.

### 3.2.3 Least Square Fitting

In order to compute the normal vector $\mathbf{n} = (n_x, n_y, n_z)$ for the point set $N_i$, we first formulate the neighbor point set as $\mathbf{A} \in \mathcal{R}^{k\times 3}$. $\mathbf{b} \in \mathcal{R}^{k\times 1}$ is a constant vector.

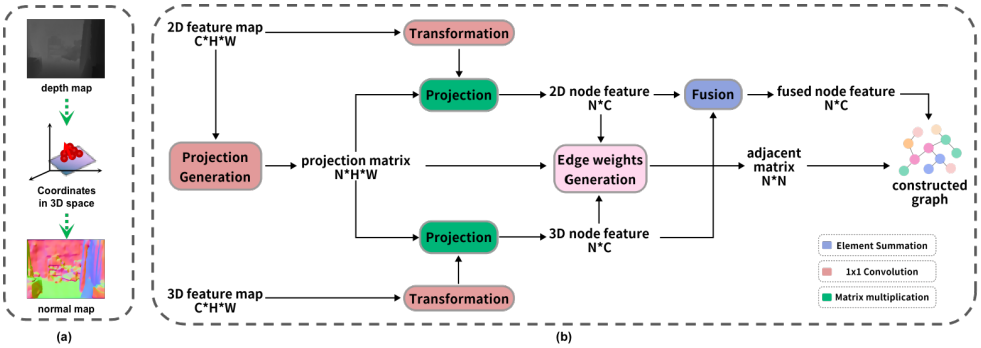


**Fig. 4** (a): Illustration of depth encoding process. We first project depth map to point cloud; then, the least square fitting is adopted to compute the normal vector of each point; finally, we get the final normal map depicting the object surface normal tendencies. (b): Details of graph construction process. The graph construction module takes feature map from two modalities as its input and output fused graph, containing node feature and adjacent matrix. Note that the fusion operation can be a simple summation or concatenation, which will be discussed in 4.3 and there are serval options of generating edge weights, each will be introduced in 3.3.4

Therefore, the normal-vector should satisfy:

$$\mathbf{An} = \mathbf{b}, s.t. \|\mathbf{n}\|_2^2 = 1 \tag{2}$$

We adopt the least square method to find the optimal normal vector via minimizing $\|\mathbf{An} - \mathbf{b}\|_2^2$, formulated as:

$$\mathbf{n} = \frac{(\mathbf{A}^T\mathbf{A})^{-1}\mathbf{A}^T\mathbf{1}}{\|(\mathbf{A}^T\mathbf{A})^{-1}\mathbf{A}^T\mathbf{1}\|_2^2} \tag{3}$$

where $\mathbf{1} \in \mathcal{R}^k$ is a vector with all 1 elements.

In summary, by projecting the depth data into point cloud, we get the point set $S$; by define neighborhood number, we get the k-nearest neighbor set $N_i^k$ for $(u_i, v_i)$; by using least square fitting, we get the normal vectors $\mathbf{n}$ for all points, which can be saved as a three-channel normal map. Note that selecting different neighborhood numbers lead to different normal maps: as k grows larger, the normal map is more "smoothed" and losses details. Empirically, we can get better results when $k = 9$. After that, two semantic segmentation networks with different backbones that have been pre-trained on Image-Net are adopted for the initial segmentation.

## 3.3 Graph Construction

The Graph Construction Module takes the feature maps from two modalities as its input, and output the constructed graph with node features and the adjacent matrix. Note that the input of this module is the output of the encoder-decoder, whose backbone has been pre-trained on Image-Net so that the output feature map can have initial semantic information.

The goal of this module is, on one hand, to assemble pixels that have similar semantic features together and transform them to a node in the graph; on the other hand, to fuse RGB-D and depth via transforming them into one graph. It is composed of four steps: 1), generate projection matrix; 2), transform the feature from coordinate space to semantic space; 3), aggregate node features from two modalities; and 4), generate the adjacent matrix. Fig 4(b) illustrate the overall process. Details will be described in the following 4 sections.

### 3.3.1 Projection Matrix Generation

The projection matrix is derived from the 2D feature map and is mainly used to project the pixel features in the coordinate space into the node features in the semantic space, during which pixels that have similar features in the coordinate space are assigned to the same node in the semantic space. Formally, this module takes the initial feature map $X \in \mathcal{R}^{C\times H\times W}$ as input, and output the projection matrix $P \in \mathcal{R}^{N\times H\times W}$. Denoted as

$$P = F_g(X) \tag{4}$$

The most intuitive instantiation of $F_g$ is to apply region growth method on the feature map. But in practice, this is neither differentiable nor multiply-able, which means it takes much more time than convolution operations and cannot be back-propagated. Inspired by previous work [43], we consider this process as a assignment computing task and the $F_g$ can be a $1 * 1$ convolution layer, whose input channel and output channel are $C$ and $N$, respectively.

Ideally, the transformed node features should, on one hand, make sure each pixel in the coordinate space will be assigned to one node in the semantic space; on the other hand, be inter-node compact and intra-node distinct, meaning that the assignment process should consider the similarities semantically and positionally. But in practice, generating projection matrix via one single convolution layer cannot satisfy two goals due to the spatial-agnostic characteristic inherited from convolution operations.

We discover that the projection matrix tends to be sparse as the training goes on. Shown in Fig 6(a), at the initial iteration, the blue dots are evenly distributed over the entire image, indicating that each pixel has one node as primarily assigned. But as training proceeds, the proportion of blue dots in the whole image quickly dropped, indicating that pixels in the blue area are assigned to multiple nodes while pixels in the white area are not assigned to any nodes. We name this phenomenon as **Biased-Assignment Problem**. Such phenomena may further lead some features to be redundant while others are missing.

As we further analysis the reason why this phenomenon occurs is that as the training goes, we discover that the encoder-decoder networks can correctly categorize easy pixels, whose predicted vectors are similar to one-hot. Thus, Graph neural networks focus on the regions that are difficult for the encoder-decoder networks to discriminate, whose predicted vectors are similar to a uniform distributed vector. Therefore, we can take the Graph Neural Network as a process of hard pixel mining process and another function of the projection matrix lies in finding these difficult pixels. Inspired by [41], we use a Kullback–Leibler Loss function to minimize the divergence between projection matrix $P$ and a uniform-distributed matrix. Mathematically, it can be formed

as:

$$L_{KL} = Kullback - Leibler(P, I) \tag{5}$$

where $I$ is a uniform-distributed matrix shaping like $P$.

Another attempt is that replacing the soft-assignment with hard-assignment, after which the pixels will be and only be assigned to one node based-on the likelihood in the projection matrix. In other words, the elements in the projection matrix are either 1 or 0, indicating current pixel is assigned to one particular node or not. Experiments show that such soft-to-hard transition is not as effective as the KL-Loss effect.

### 3.3.2 Feature Transformation

Considering that a higher node feature dimension causes an exponential increase in computation during the graph convolution stage, we use a feature transformation module to reduce dimension. It takes feature maps in the coordinate space from two modalities as its input, output the transformed feature maps, denoted as

$$Z = F_t(X) \tag{6}$$

Note that such transformations are exactly the same on two branches, only with different parameters. In practice, we use a linear function to convert the high dimensional feature into a lower one. There exists a balance between the computational complexity and the performance, which will be discussed in Section 4.3.

### 3.3.3 Project and Fuse

This module takes the transformed features from two modalities $Z$ and the projection matrix $P$ as its input, output the projected and fused node feature. For the projection part, we get projected node feature via a simple matrix multiplication:

$$V = Z \cdot P \tag{7}$$

The similar feature transformation process is employed on the 3D branch, only that the projection matrix is inherited from the RGB-D branch, not generated from 3D feature map like equation 4 did. In other words, for a sampled RGB-D image and depth map, there only exist one projection matrix. Designing like this, on one hand, is for the homogeneity of two graph, which makes it easy to fuse two modalities via a simple concatenation; on the other hand, is because that RGB-D images are rich in texture so we can use RGB-D to "lead" and the depth to "supplement". For the fusion part, we simply apply a summation to get the final node feature matrix.

### 3.3.4 Adjacent Matrix Generation

Most existing methods generate adjacent matrix based-on the similarity of node features, which makes the GNNs focus on the hidden semantic relations and ignore the region positional information. Instead, we argue that positional information equally plays an important role in pixel-wise semantic segmentation, and such neglect in graph

reasoning process may hurt the performance. Therefore, our edge generation module takes the projection matrix as its input and output two symmetric adjacent matrix, considering that the graph is a non-directional graph. Each adjacent matrix indicates node similarities semantically and positionally, named as semantic-aware adjacent matrix and locality-aware adjacent matrix, denoted as $A_s, A_l \in \mathcal{R}^{N \times N}$, respectively.

For the semantic-aware adjacent matrix, we follow the existing approach where the edge weights are generated based on the semantic similarity. Specifically, we multiply the node feature matrix directly with its transpose. Therefore, **Semantic-aware edge weights** can be obtained. We take $v_i$ as the node feature embedding computed from Equation 7, so the so semantic-aware edge weight between $i$-th and $j$-th node can be computed in a simple multiplication:

$$w_{s_{ij}} = v_i \cdot {v_j}^T \tag{8}$$

For the locality-aware adjacent matrix, considering there are $N$ layers in the projection matrix and each layer denotes the possibility of assigning $H \times W$ pixels to current node, we argue that each $H \times W$ shaped 2D matrix can be used to represent the positional information of each node and the whole projection matrix can be used to represent the positional information of all nodes. Here we propose two different approaches to generate locality-aware adjacent.

The most intuitive approach is to multiply the projection matrix directly with its transpose, the resulting adjacency matrix can reflect the similarity in position between two nodes, just like Eq.8 did. Although experiments in Section4.3 shows such approach can achieve competitive results, directly use a high-dimensional vector is neither explainable nor visualizable, and may be not sufficient to monitor the compactness of each region whereas redundant to describe the region location.

To model location information into a more visualizable form, we introduce $M \in \mathcal{R}^{N \times 3}$ to represent per-node positional center coordinates. Fig 5 shows an example of how one layer of the projection matrix generate its corresponding node positional vector in 2D and 3D branch and the visualization of computed positional coordinates in 2D and 3D space. In other words, take 3D branch for example, the positional encoding process can transform a $H * W$ shaped assignment matrix into a $1 * 3$ shaped positional vector, denoting the region's location in the 3D space. But in practice, this computation process is not only time-consuming but also unable to be back-propagated. Therefore, we apply a linear transformation on the projection matrix $P$ to generated the region center matrix $M_c \in \mathcal{R}^{N \times 3}$. To supervise this process, we use Mean Square Error (MSE) to minimize the distances between transformed coordinates and its corresponding ground truth. It can be formulated as:

$$L_{MSE} = MSE(M_g, M_c) \tag{9}$$

Note that the time-consuming computing only happens at the training stage and is used to supervise the transformation. Hence, the **Locality-aware edge weights** can be obtained by computing the Euclidean distance between each coordinates. We take $(x_i, y_i, z_i)$ as the $i$-$th$ node positional encoding so locality-aware edge weight between

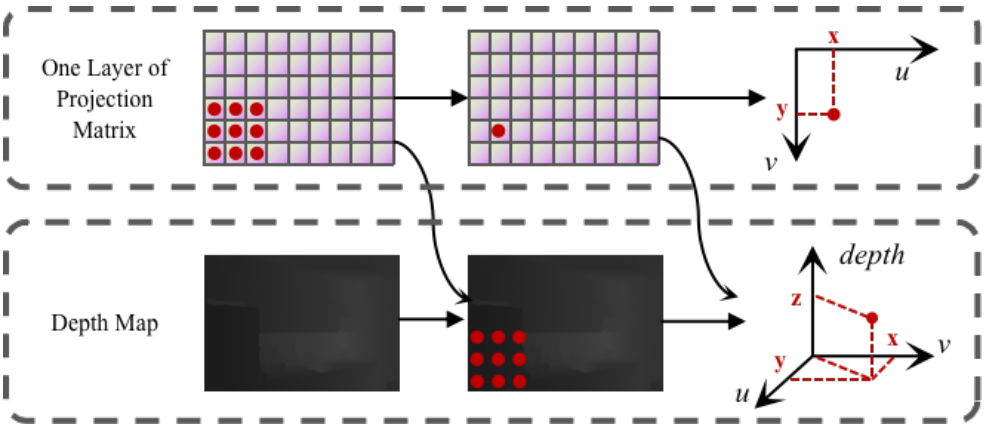


**Fig. 5** Illustration and visualization of 2 types of positional encoding process for one layer in the projection matrix. For 2D branch, we take the projection matrix as its input and for 3D branch, both projection matrix and the depth map are required. The output are computed positional encoding, where $x$ and $y$ is coordinates of region center in 2D space and $z$ is the average depth value of current region.

*i-th* and *j-th* node can be formulated as:

$$w_{l_{ij}} = \frac{1}{Euclid(i,j)} \tag{10}$$

## 3.4 Graph Neural Networks

The Graph Neural Networks Module takes fused node features $V$ and the adjacent matrix $E$ as its input, output the updated node features. The aim of this module is to conduct feature learning on the fused graph, furthermore, to capture relations in the semantic space as well as positional attributes in the coordinate space. This semantic capturing and reasoning process can be formulated as:

$$\tilde{V} = F_n(V, W) \tag{11}$$

where $F_g$ can be Graph Reasoning or Graph Convolution. In practice, we adopt Graph Convolution Networks [44] to update node features based on the neighbor nodes. Formally, for the input node embedding $h_v$ with its neighbors embedding $h_u$, where $u = \mathcal{N}(v_i)$, a graph convolutional layer performs message computing and feature aggregation operations and output the updated embedding of node $\tilde{h_v}$.

To preserve features from node itself, different message computation will be performed on node itself and its neighbors:

$$m_v = W_S(h_v) \tag{12}$$

$$m_u = AGG[W_N(h_u)] \tag{13}$$

where $W_S$ and $W_N$ can be linear transformation upon the node embedding, and $AGG$ can be a simple averaging, maximization or summation to aggregate neighbors' feature. Then, a summation is applied to get updated node feature:

$$\tilde{h_v} = \sigma(SUM[m_v, m_u]) \tag{14}$$

where $\sigma$ is an activation layer and is used to add network's nonlinearity. Note that the parameters involved are completely learnable and multiple layers can be stacked to increase the range of neighborhoods.

### 3.5 Graph Re-projection

Our goal at this stage is to transfer updated node feature $V_{new} \in \mathcal{R}^{N \times D}$ back to the coordinate space. The re-projection process can be seen as a reverse version of projection module. In practice, we discover that the projection matrix generated in the graph construction process can be re-used here. Specifically, the re-projection matrix is the transpose of the projection matrix, denoted as $Q = P^T = \{q_1, q_2, ..., q_N\} \in \mathcal{R}^{H*W \times N}$. Therefore, the updated feature map can be obtained via a simple matrix multiplication

$$\tilde{Z} = Q \cdot \tilde{V} \tag{15}$$

Note that there is a feature dimension shift to transform the feature just like Section 3.3.2 did. It can be formulated as $\tilde{X} = \tilde{Z} \cdot T'$, during which introduced no extra parameters and have no negative effect on the final accuracy.

Finally, Cross Entropy Loss is used to supervise the output feature map:

$$L_{CE} = CrossEntropy(\tilde{X}, Y) \tag{16}$$

where $Y$ is the corresponding ground truth.

### 3.6 Loss Function

Th loss function is composed of 3 parts, as Fig 3 shows. Firstly, the Cross Entropy is used to reduce the pixel-wise loss between the final output mask and the ground-truth label. Secondly, KL-Divergence is used to avoid the Biased-Assignment issue caused by projection matrix. Lastly, Mean Square Error is used to supervise the positional compactness of each region. Formally, the total loss function is computed as:

$$Loss = L_{CE} + \alpha \cdot L_{KL} + \beta \cdot L_{MSE} \tag{17}$$

where $L_{KL}$ and $L_{MSE}$ have beed introduced in Equation 5 and 9 and 16. Note that in Fig 3, we only show the $L_{KL}$ and $L_{CE}$. It is because that it $L_{MSE}$ is only one of many ways to generate adjacency matrix, and when we use other generation methods it is no longer necessary.

In summary, given a feature map $X \in \mathcal{R}^{H \times W \times C}$, we first generate the projection matrix $P$ and transform $X$ into node feature $V$; then, edge weights are generated based

**Table 1** Ablation Study on 2D branch

| | improvements on $P$ | | | choices on edge weights generation | | | choices on GNNs | | mIOU(%) | ↑ (%) |
|---|---|---|---|---|---|---|---|---|---|---|
| | KL-Loss | Soft | Hard | from V | from $P$ | from centroids | Graph Reasoning | Graph Convolution | | |
| 2D baseline | | Y | | Y | | | Y | | 44.3 | - |
| baseline+ | Y | Y | | Y | | | Y | | 45.6 | 1.3 |
| baseline+ | Y | | Y | Y | | | Y | | 45.8 | 1.5 |
| baseline+ | Y | | Y | | Y | | Y | | 46.0 | 1.7 |
| baseline+ | Y | | Y | | | Y | Y | | 46.3 | 2.0 |
| baseline+ | Y | | Y | | | Y | | Y | 47.0 | 2.3 |

**Table 2** Ablation Study on fusion choice

| | aggregation | | input choice of 3D branch | | | mIOU(%) | ↑ (%) |
|---|---|---|---|---|---|---|---|
| | Sum | Cat | depth map | normal map | HHA | | |
| 3D baseline | | Y | Y | | | 48.9 | - |
| baseline+ | Y | | Y | | | 49.5 | 0.6 |
| baseline+ | Y | | | Y | | 50.6 | 1.7 |
| baseline+ | Y | | | | Y | 50.8 | 1.9 |

**Table 3** Comparison-with-SOTAs on NYU-v2

| Method | Backbone | 3D data | mAcc(%) | mIOU(%) |
|---|---|---|---|---|
| FCN-16s[15] | VGG16*2 | HHA | 46.1 | 34.0 |
| RDF-Net* [25] | R50*2 | depth | 60.4 | 47.7 |
| LSD-Net [26] | VGG16*2 | HHA | 60.7 | 45.9 |
| Malleable 2.5D [30] | R50 | depth | - | 48.8 |
| 2.5D-Convolution [48] | R101*2 | HHA | - | 49.1 |
| ShapeConv [31] | R50*2 | HHA | 59 | 47.3 |
| Bi-directional [49] | R50*2 | HHA | - | 50.4 |
| InverseForm [50] | R101 | - | - | 53.1 |
| Co-Attention* [51] | R50*2 | depth | 62.6 | 49.6 |
| RGB-X [34] | MiT-B2 | HHA | - | 52.0 |
| Ours | R50+R18 | depth | 61.9 | 49.5 |
| | R50+R18 | normal | 62.7 | 50.6 |
| | R50+R18 | HHA | 63.0 | 50.8 |

on the projection matrix, depth map and node feature; after that, we constructed graph $\mathcal{G} = (V, E)$ and perform Graph Convolution on it; lastly, the updated node feature are re-projection back to the feature map. Note that the proposed method is applied on the output of the encoder-decoder module, which have beed pre-trained on ImageNet so the initial output feature map has semantics on some degree. We pre-define the number of the node in the graph as $N$, and the feature dimension of each node as $D$, whose effect will be further discussed in Section 4.3.

# 4 Experiments

## 4.1 Datasets and Metrics

The existing RGB-D indoor dataset is challenging due to complex layouts and severe occlusions. We carry out comprehensive experiments on NYUDv2-40 [52] and SUN RGB-D [53] to evaluate the effectiveness of the proposed method. **NYUDv2** is a dataset composed of video sequences from a variety of indoor scenes as recorded by both the RGB and Depth cameras from the Microsoft Kinect. It contains 1,449 RGB-D samples, and each sample is composed of RGB image, depth map, camera parameter matrix, and its semantic label mask, where all pixels are labeled with 13 and 40 classes, respectively. We adopt the most popular setting that 795 images are for training and 654 images are for testing. **SUN RGB-D Dataset** is composed of 10, 335 RGB-D samples, coming from existing RGBD datasets [52] [54] [55] as well as newly captured data. We use the standard training/testing split [53] of 5285/5050 in our

experiment with 37-category semantic labels. Mean Accuracy (MeanAcc) and Mean Region Intersection Over Union (MeanIoU) are used for the per-class evaluation.

## 4.2 Implementation Details

We employ the classic semantic segmentation network, that is, DeepLabV3 with ResNet50, as our backbone, which have been pre-trained on ImageNet. The proposed method is appended directly at the end of the final output layer. The networks are updated using Adam, where the initial learning rate is 0.01, and the weight decay is 0.0002. The experiments are implemented with PyTorch and with one NVIDIA RTX 3090 GPU. The batch size is set to be 4.

## 4.3 Ablation Study

We compare results with different settings to evaluate the effectiveness of the proposed modules, which can be categorized as two types: the constraints on the projection matrix and how the edge weights are generated for 2D branch, the fusion choice for 3D branch. All these experiments are conducted on NYUv2 dataset and evaluated by mIOU.

For 2D branch, we take the widely used DeepLabV3+ with backbone ResNet50 as our RGB baseline. To alleviate the Biased-Assignment issue, we change the assignment type and add a KL-loss which have been introduced in section 3.3. As shown in the first three lines of Table 1, we can see that using a KL-Divergence Loss on the projection matrix can bring a 1.2% improvement, changing the assignment from soft to hard has a 0.2% increasement, whereas the combination of two parts can bring a total 1.3% improvement. To find the optimal way of generating edge weights, we compare three different approaches and find that generating edge weights from region centroids achieves the highest mIOU. We also compare the results of different graph neural networks, deploying a GCN layer instead of the original Graph Reasoning layer can boost a 0.5% improvement. It is worth noting that when we take the inference time into consideration, generating edge weights from projection matrix can achieve competitive mIOU whereas using much less parameters.

For the fusion branch, we average the predictions of two parallel DeepLabV3+ as our RGB-D baseline. As shown in Table 2, the simple summation of two feature maps not only outperforms the concatenation on the final prediction but also needs relatively smaller number of parameters. The input of 3D branch can be depth map, normal map, and HHA map. The latter two achieve competitive results while directly using depth map as input has limited improvements. This validate our assumption that traditional CNN operators are not good at capturing depth tendencies and converting the depth map to normal map or HHA map can alleviate this problem.

## 4.4 Comparison with State-of-the-Art Methods

We compare the proposed approach with previous methods with similar settings on two public datasets. Table 3 and 4 show the mAcc and mIOU of different methods on NYUDv2 and SUN RGB-D. We also show their choice of 3D data input type and the choice of backbone each method has adopted, since these settings have a great

**Table 4** Comparison-with-SOTAs on SUN RGB-D

| Method | Backbone | 3D data | mAcc(%) | mIOU(%) |
|---|---|---|---|---|
| FCN-32s [15] | VGG16*2 | depth | 41.13 | 29.0 |
| FuseNet [24] | VGG16*2 | depth | 48.46 | 37.76 |
| LSD-Net [26] | VGG16*2 | HHA | 58.0 | - |
| RDF-Net* [25] | R152*2 | depth | 60.1 | 47.7 |
| 2.5D-Convolution [48] | R101*2 | HHA | - | 48.2 |
| RGBxD [23] | R101 | HHA | 58.8 | 47.7 |
| ESA-Net [56] | R50*2 | depth | - | 48.31 |
| ShapeConv [31] | R50*2 | HHA | 56.8 | 46.3 |
| Co-Attention* [51] | R50*2 | depth | 59.0 | 48.1 |
| Co-Attention* [51] | R101*2 | depth | 60.5 | 49.3 |
| Ours | R50+R18 | depth | 58.6 | 47.9 |
| | R50+R18 | normal | 59.7 | 49.1 |
| | R50+R18 | HHA | 60.1 | 49.3 |

impact on the final results. It can be observed from the tables that with same backbone choice and 3D data selection, our proposed approach achieves competitive results and replacing the input of 3D branch with HHA further boost the performance.

Worth to mention that when the 3D data are both depth maps, the performance of Co-attention [51] is slightly better than ours. This is because that on one hand, [51] builds sound interaction between RGB and depth features, whereas we just deploy a simple summation guiding by texture features; on the other hand, [51] adopts a multi-scale loss function as we have indicated with "*" in the table, whereas we only calculate a single final output loss. When the 3D data are both HHA, RGB-X [34] outperforms the rest methods with a large margin. We argue that because RGB-X is a cross-modal fusion framework, which utilizes the advantages of vision-transformer, resulting in a strong long-range context exchange at a global level.

As shown in Table 3, some of the methods achieves noticeable results without doubling the backbone. Malleable 2.5D [30] designs delicate convolutional operations for feature learning on depth data, resulting competitive results using depth maps. InverseForm [50] presents a novel boundary-aware loss term for semantic segmentation, which achieves similar purpose on the boundary-fixing level compared with our method, but the different part is that we also aim to learn the regions dependencies, not just the boundary improvement. RGBxD [23] is an early fusion method, fusing RGB and 3D data in the input level. Therefore, there does not exist backbone doubling.

In summary, the strength of our method is mainly at two aspects. Firstly, we encode the depth map as an object surface normal map, which enables us to adopt a lighter-weight backbone network for 3D feature extraction. Secondly, the adoption of pixel-node-pixel pipeline and its followed-up improvements enables the network "reason like a human". In other words, it can learn relations on the region level, not just pixel level.

## 4.5 Further Analysis

To further analyze the impact of transformation module, we conduct experiments using the same settings except different three parts: the node number in each graph, the feature dimension of each number, and the existence of feature transformation

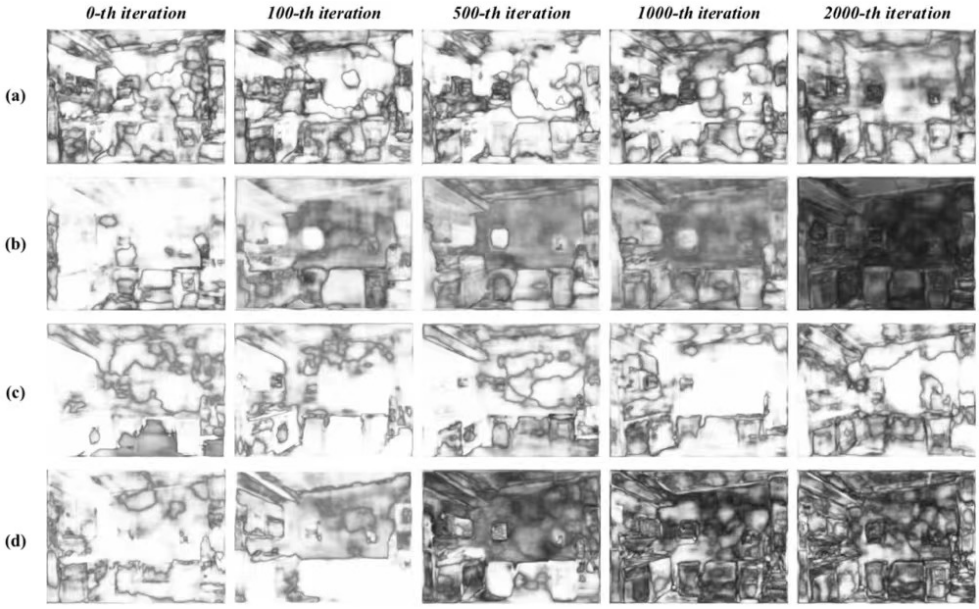


**Fig. 6** Illustration of the Biased-Assignment and the effectiveness of the proposed KL-Loss. All images are from the same sample. Each column shows the assignment at the same training stage with different settings: (a) hard-assignment without the KL-Loss constraints; (b) hard-assignment with the KL-Loss constraints; (c) soft-assignment without the KL-Loss constraints; (d) soft-assignment with the KL-Loss constraints. Each row shows the assignment with the same setting at different training stages: 0-$th$, 100-$th$, 500-$th$, 1000-$th$, 2000-$th$ iteration(s).

module. We set a threshold at the choice of node number and feature dimension, which means excessive increasement in model complexity may have a negative impact on the model performance. The existence of the feature transformation can reduce the number of parameters involved in the GNN process, but it slightly decreases the final performance.

As a crucial component of our pipeline, the projection matrix plays an important part in transforming features from pixels to graph nodes. Yet, few researchers have analyzed it in previous works. To dive into the projection matrix and evaluate the effectiveness of the constraints we added, we randomly pick one sample from the dataset and visualize the assignment at different layers as well as different training stages. Considering that the original high-dimensional projection matrix is not easy to visualize, we pick its maximum in the channel dimension to get a single channel matrix, which can be easily viewed in grayscale. As Fig 6 shows, the larger maximum value we obtained is, the more "confident" our network is to assign the current pixel to one certain node, and the brighter this pixel will be. Just like we previously discussed in Sec 3.3.1, another direction to understand the function of the projection matrix is the hard-pixel mining aspect. Combining the observation we get from Fig 6, we can discover that the deployment of the KL-Loss makes the network less confident, so more pixels are considered as "difficult pixels", on which the learning of the graph neural network can be carried out better.

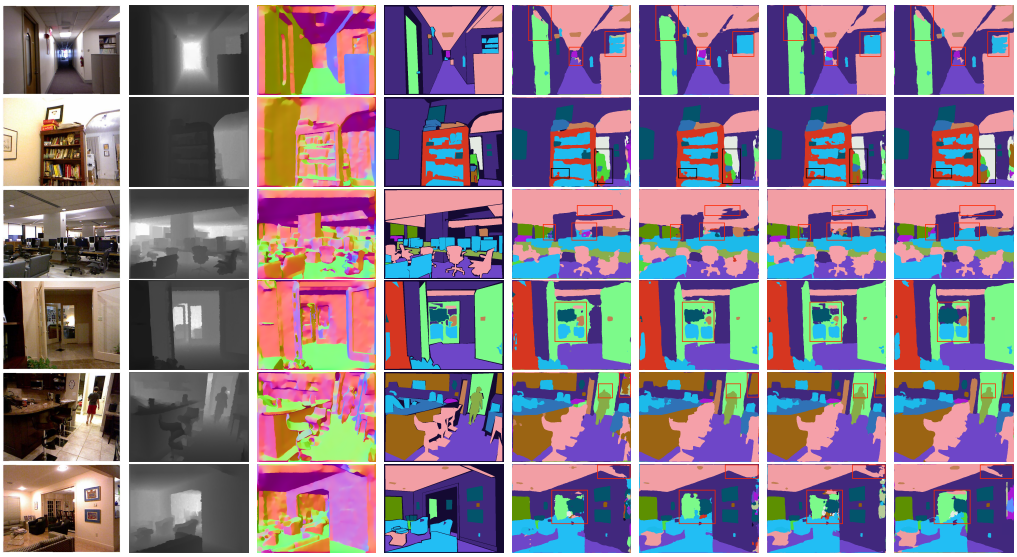

(a) RGB (b) depth map (c) normal map (d) Groundtruth (e) 2D Baseline (f) 2D Ours (g) 3D Baseline (h) 3D Ours

**Fig. 7** Quantitative visualization. The improved segmented regions are marked with red (or black for second row) rectangles. Noticeably, the proposed module on the 2D branch can alleviate the emergence of irregular patches. Incorporating 3D data can increase the consistency of object surface in the segmented results and further boost the final performance. Best view in color.

# 5 Visualization

We sample six set of data from the testing set of NYUDv2. As Fig 7 shows, comparing column(e) with (f), (g) with (h), we can observe our improvements, i.e, constraints on the projection matrix and positional encoding process. The proposed module can reduce the presence of irregular patches. Comparing column (b) with (c), we can observe that the 3-channel normal maps are richer in texture compared with 1-channel depth map and shows the consistency of the surface of the object in a more direct way. Comparing column (e) with (g), (f) with (h), we can observe that feature extracting on normal maps can improve geometric consistency and further boost the segmentation results. But there still exist irregular patches where semantic labels are missing due to poor lightening condition and long distance, where our performance slightly dropped but still preserve reasonable semantic consistency.

# 6 Conclusion

How to make the neural network "reason like a human" is still an area that remains to be studied. In this paper, we propose a RGB-D semantic segmentation method that empower the network to learn dependencies on arbitrary regions and further alleviate the counter-intuitive segmentation problem. A depth encoding method is applied to explicitly extract object surface geometric feature, which is beneficial for the

following feature learning process. The graph-based pipeline is adopted to reasonably fuse features from two modalities in a texture-prior style. We have demonstrated that our approach is effective on two public datasets. In the future work, how to more efficiently incorporate node positional as well as semantic information into graph data, and how to improve graph neural networks the are yet to be further studies.

# References


[1] Mo, Y., Wu, Y., Yang, X., Liu, F., Liao, Y.: Review the state-of-the-art technologies of semantic segmentation based on deep learning. Neurocomputing **493**, 626–646 (2022)

[2] Wei, Y., Xiao, H., Shi, H., Jie, Z., Feng, J., Huang, T.S.: Revisiting dilated convolution: A simple approach for weakly-and semi-supervised semantic segmentation. In: Proceedings of the IEEE Conference on Computer Vision and Pattern Recognition, pp. 7268–7277 (2018)

[3] Simonyan, K., Zisserman, A.: Very deep convolutional networks for large-scale image recognition. arXiv preprint arXiv:1409.1556 (2014)

[4] Hu, J., Shen, L., Sun, G.: Squeeze-and-excitation networks. In: Proceedings of the IEEE Conference on Computer Vision and Pattern Recognition, pp. 7132–7141 (2018)

[5] Wang, X., Girshick, R., Gupta, A., He, K.: Non-local neural networks. In: Proceedings of the IEEE Conference on Computer Vision and Pattern Recognition, pp. 7794–7803 (2018)

[6] Yuan, Y., Chen, X., Wang, J.: Object-contextual representations for semantic segmentation. In: European Conference on Computer Vision, pp. 173–190 (2020). Springer

[7] Li, X., Zhao, H., Han, L., Tong, Y., Tan, S., Yang, K.: Gated fully fusion for semantic segmentation. In: Proceedings of the AAAI Conference on Artificial Intelligence, vol. 34, pp. 11418–11425 (2020)

[8] Carion, N., Massa, F., Synnaeve, G., Usunier, N., Kirillov, A., Zagoruyko, S.: End-to-end object detection with transformers. In: European Conference on Computer Vision, pp. 213–229 (2020). Springer

[9] Dosovitskiy, A., Beyer, L., Kolesnikov, A., Weissenborn, D., Zhai, X., Unterthiner, T., Dehghani, M., Minderer, M., Heigold, G., Gelly, S., et al.: An image is worth 16x16 words: Transformers for image recognition at scale. arXiv preprint arXiv:2010.11929 (2020)

[10] Wang, C., Wang, C., Li, W., Wang, H.: A brief survey on rgb-d semantic segmentation using deep learning. Displays **70**, 102080 (2021)

[11] Liu, M., Schonfeld, D., Tang, W.: Exploit visual dependency relations for semantic segmentation. In: Proceedings of the IEEE/CVF Conference on Computer Vision and Pattern Recognition, pp. 9726–9735 (2021)

[12] Wu, Y., Zhang, G., Gao, Y., Deng, X., Gong, K., Liang, X., Lin, L.: Bidirectional graph reasoning network for panoptic segmentation. In: Proceedings of the IEEE/CVF Conference on Computer Vision and Pattern Recognition, pp. 9080–9089 (2020)

[13] Zhou, L., Liu, Y., Bai, X., Wang, X., Wang, C., Zhang, L., Gu, L.: Relation-aware reasoning with graph convolutional network. In: International Conference on Image and Graphics, pp. 52–64 (2021). Springer

[14] Wang, C., Fu, H., Ling, C.X., Du, P., Ma, H.: Region-based global reasoning networks. In: Proceedings of the AAAI Conference on Artificial Intelligence, vol. 34, pp. 12136–12143 (2020)

[15] Long, J., Shelhamer, E., Darrell, T.: Fully convolutional networks for semantic segmentation. In: Proceedings of the IEEE Conference on Computer Vision and Pattern Recognition, pp. 3431–3440 (2015)

[16] Ronneberger, O., Fischer, P., Brox, T.: U-net: Convolutional networks for biomedical image segmentation. In: International Conference on Medical Image Computing and Computer-assisted Intervention, pp. 234–241 (2015). Springer

[17] Chen, L.-C., Papandreou, G., Kokkinos, I., Murphy, K., Yuille, A.L.: Deeplab: Semantic image segmentation with deep convolutional nets, atrous convolution, and fully connected crfs. IEEE transactions on pattern analysis and machine intelligence **40**(4), 834–848 (2017)

[18] Cheng, B., Collins, M.D., Zhu, Y., Liu, T., Huang, T.S., Adam, H., Chen, L.-C.: Panoptic-deeplab: A simple, strong, and fast baseline for bottom-up panoptic segmentation. In: Proceedings of the IEEE/CVF Conference on Computer Vision and Pattern Recognition, pp. 12475–12485 (2020)

[19] Wang, X., Girshick, R., Gupta, A., He, K.: Non-local neural networks. CVPR (2018)

[20] Fu, J., Liu, J., Tian, H., Li, Y., Bao, Y., Fang, Z., Lu, H.: Dual attention network for scene segmentation. In: Proceedings of the IEEE Conference on Computer Vision and Pattern Recognition, pp. 3146–3154 (2019)

[21] Huang, Z., Wang, X., Huang, L., Huang, C., Wei, Y., Liu, W.: Ccnet: Criss-cross attention for semantic segmentation (2019)

[22] Zhang, Y., Sidibé, D., Morel, O., Mériaudeau, F.: Deep multimodal fusion for semantic image segmentation: A survey. Image and Vision Computing **105**,

104042 (2021)

[23] Cao, J., Leng, H., Cohen-Or, D., Lischinski, D., Chen, Y., Tu, C., Li, Y.: Rgb× d: Learning depth-weighted rgb patches for rgb-d indoor semantic segmentation. Neurocomputing **462**, 568–580 (2021)

[24] Hazirbas, C., Ma, L., Domokos, C., Cremers, D.: Fusenet: Incorporating depth into semantic segmentation via fusion-based cnn architecture. In: Asian Conference on Computer Vision, pp. 213–228 (2016). Springer

[25] Park, S.-J., Hong, K.-S., Lee, S.: Rdfnet: Rgb-d multi-level residual feature fusion for indoor semantic segmentation. In: Proceedings of the IEEE International Conference on Computer Vision, pp. 4980–4989 (2017)

[26] Cheng, Y., Cai, R., Li, Z., Zhao, X., Huang, K.: Locality-sensitive deconvolution networks with gated fusion for rgb-d indoor semantic segmentation. In: Proceedings of the IEEE Conference on Computer Vision and Pattern Recognition, pp. 3029–3037 (2017)

[27] Wang, Y., Huang, W., Sun, F., Xu, T., Rong, Y., Huang, J.: Deep multimodal fusion by channel exchanging. Advances in Neural Information Processing Systems **33**, 4835–4845 (2020)

[28] Chen, S., Zhu, X., Liu, W., He, X., Liu, J.: Global-local propagation network for rgb-d semantic segmentation. arXiv preprint arXiv:2101.10801 (2021)

[29] Wang, W., Neumann, U.: Depth-aware cnn for rgb-d segmentation. In: Proceedings of the European Conference on Computer Vision (ECCV), pp. 135–150 (2018)

[30] Xing, Y., Wang, J., Zeng, G.: Malleable 2.5 d convolution: Learning receptive fields along the depth-axis for rgb-d scene parsing. In: European Conference on Computer Vision, pp. 555–571 (2020). Springer

[31] Cao, J., Leng, H., Lischinski, D., Cohen-Or, D., Tu, C., Li, Y.: Shapeconv: Shape-aware convolutional layer for indoor rgb-d semantic segmentation. In: Proceedings of the IEEE/CVF International Conference on Computer Vision, pp. 7088–7097 (2021)

[32] Jiao, J., Wei, Y., Jie, Z., Shi, H., Lau, R.W., Huang, T.S.: Geometry-aware distillation for indoor semantic segmentation. In: Proceedings of the IEEE/CVF Conference on Computer Vision and Pattern Recognition, pp. 2869–2878 (2019)

[33] Liu, Z., Qi, X., Fu, C.-W.: 3d-to-2d distillation for indoor scene parsing. In: Proceedings of the IEEE/CVF Conference on Computer Vision and Pattern Recognition, pp. 4464–4474 (2021)

[34] Liu, H., Zhang, J., Yang, K., Hu, X., Stiefelhagen, R.: Cmx: Cross-modal fusion for rgb-x semantic segmentation with transformers. arXiv preprint arXiv:2203.04838 (2022)

[35] Yao, Y., Jiang, X., Fujita, H., Fang, Z.: A sparse graph wavelet convolution neural network for video-based person re-identification. Pattern Recognition **129**, 108708 (2022)

[36] Zhao, G., Ge, W., Yu, Y.: Graphfpn: Graph feature pyramid network for object detection. In: Proceedings of the IEEE/CVF International Conference on Computer Vision, pp. 2763–2772 (2021)

[37] Shi, W., Rajkumar, R.: Point-gnn: Graph neural network for 3d object detection in a point cloud. In: Proceedings of the IEEE/CVF Conference on Computer Vision and Pattern Recognition, pp. 1711–1719 (2020)

[38] Zhang, Y., Huang, D., Wang, Y.: Pc-rgnn: Point cloud completion and graph neural network for 3d object detection. In: Proceedings of the AAAI Conference on Artificial Intelligence, vol. 35, pp. 3430–3437 (2021)

[39] Qi, X., Liao, R., Jia, J., Fidler, S., Urtasun, R.: 3d graph neural networks for rgbd semantic segmentation. In: Proceedings of the IEEE International Conference on Computer Vision, pp. 5199–5208 (2017)

[40] Chen, Y., Mensink, T., Gavves, E.: 3d neighborhood convolution: learning depth-aware features for rgb-d and rgb semantic segmentation. In: 2019 International Conference on 3D Vision (3DV), pp. 173–182 (2019). IEEE

[41] Li, Y., Gupta, A.: Beyond grids: Learning graph representations for visual recognition. Advances in Neural Information Processing Systems **31** (2018)

[42] Liang, X., Hu, Z., Zhang, H., Lin, L., Xing, E.P.: Symbolic graph reasoning meets convolutions. Advances in Neural Information Processing Systems **31** (2018)

[43] Chen, Y., Rohrbach, M., Yan, Z., Shuicheng, Y., Feng, J., Kalantidis, Y.: Graph-based global reasoning networks. In: Proceedings of the IEEE/CVF Conference on Computer Vision and Pattern Recognition, pp. 433–442 (2019)

[44] Kipf, T.N., Welling, M.: Semi-supervised classification with graph convolutional networks. arXiv preprint arXiv:1609.02907 (2016)

[45] Han, K., Wang, Y., Guo, J., Tang, Y., Wu, E.: Vision gnn: An image is worth graph of nodes. arXiv preprint arXiv:2206.00272 (2022)

[46] Wei, L., Zhao, H., He, Z.: Designing the topology of graph neural networks: A novel feature fusion perspective. In: Proceedings of the ACM Web Conference 2022, pp. 1381–1391 (2022)

[47] Yin, Z., Shi, J.: Geonet: Unsupervised learning of dense depth, optical flow and camera pose. In: Proceedings of the IEEE Conference on Computer Vision and Pattern Recognition, pp. 1983–1992 (2018)

[48] Yajie, X., Jingbo, W., Xiaokang, C., Gang, Z.: 2.5d convolution for rgb-d semantic segmentation. In: IEEE International Conference on Image Processing, pp. 1410–1414 (2019). IEEE

[49] Chen, X., Lin, K.-Y., Wang, J., Wu, W., Qian, C., Li, H., Zeng, G.: Bi-directional cross-modality feature propagation with separation-and-aggregation gate for rgb-d semantic segmentation. In: European Conference on Computer Vision, pp. 561–577 (2020). Springer

[50] Borse, S., Wang, Y., Zhang, Y., Porikli, F.: Inverseform: A loss function for structured boundary-aware segmentation. In: Proceedings of the IEEE/CVF Conference on Computer Vision and Pattern Recognition, pp. 5901–5911 (2021)

[51] Zhou, H., Qi, L., Huang, H., Yang, X., Wan, Z., Wen, X.: Canet: Co-attention network for rgb-d semantic segmentation. Pattern Recognition **124**, 108468 (2022)

[52] Silberman, N., Hoiem, D., Kohli, P., Fergus, R.: Indoor segmentation and support inference from rgbd images. In: European Conference on Computer Vision, pp. 746–760 (2012). Springer

[53] Song, S., Lichtenberg, S.P., Xiao, J.: Sun rgb-d: A rgb-d scene understanding benchmark suite. In: Proceedings of the IEEE Conference on Computer Vision and Pattern Recognition, pp. 567–576 (2015)

[54] Janoch, A., Karayev, S., Jia, Y., Barron, J.T., Fritz, M., Saenko, K., Darrell, T.: A category-level 3d object dataset: Putting the kinect to work. In: Consumer Depth Cameras for Computer Vision, pp. 141–165. Springer, ??? (2013)

[55] Xiao, J., Owens, A., Torralba, A.: Sun3d: A database of big spaces reconstructed using sfm and object labels. In: Proceedings of the IEEE International Conference on Computer Vision, pp. 1625–1632 (2013)

[56] Seichter, D., Köhler, M., Lewandowski, B., Wengefeld, T., Gross, H.-M.: Efficient rgb-d semantic segmentation for indoor scene analysis. In: 2021 IEEE International Conference on Robotics and Automation (ICRA), pp. 13525–13531 (2021). IEEE